

Ionic-Wind-Enhanced Raman Spectroscopy without Enhancement Substrates

Qingyou Liang,* Xiangjun Gong,* Jinchao Liu, Changming Ke, Jie Dong, Guosheng Song, Pu Feng, Huakang Yu, Xianfeng Yang,* Jie Cui, Chunlin Deng,* Zhiyuan Li, Shi Liu,* and Guangzhao Zhang



Cite This: *Anal. Chem.* 2023, 95, 1318–1326



Read Online

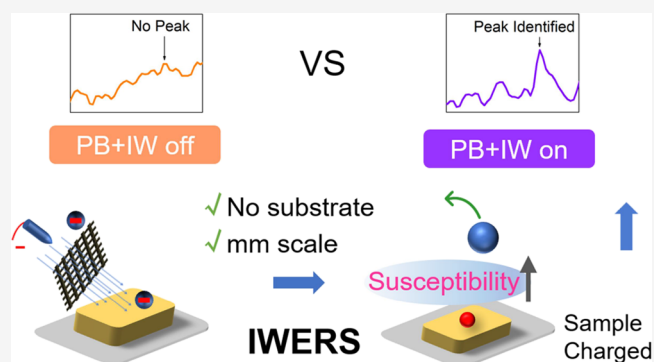
ACCESS |

Metrics & More

Article Recommendations

Supporting Information

ABSTRACT: Raman spectra are often masked by strong fluorescence, which severely hinders the applications of Raman spectroscopy. Herein, for the first time, we report ionic-wind-enhanced Raman spectroscopy (IWERS) incorporated with photobleaching (PB) as a noninvasive approach to detect fluorescent and vulnerable samples without a substrate. In this study, ionic wind (IW) generated by needle-net electrodes transfers charges to the sample surface in air on the scale of millimeters rather than nanometers in surface-enhanced Raman spectroscopy. Density functional theory calculations reveal that the ionic particles in IW increase the susceptibility of the sample molecules, thus enhancing the Raman signals. Meanwhile, the incorporation of IW with PB yields a synergistic effect to quench fluorescence. Therefore, this approach can improve the signal-to-noise ratio of Raman peaks up to three times higher than that with only PB. At the same time, IWERS can avoid sample pollution and destruction without substrates as well as high laser power. For archeological samples and a red rock as an analogue to Mars geological samples, IWERS successfully identified weak but key Raman peaks, which were masked by strong fluorescence. It suggests that IWERS is a promising tool for characterizations in the fields of archeology, planetary science, biomedicine, and soft matter.



INTRODUCTION

Raman spectroscopy is based on inelastic light scattering^{1–3} and is often masked by strong fluorescence in daily acquisition since the cross section of fluorescence is much higher than that of Raman. Fluorescence interference has been one of the main challenges for the Raman technique over half a century.^{4–6} Numerous effects have been reported to extract Raman signals in the presence of fluorescence,^{7–11} including changes in the excitation wavelength,¹² photobleaching (PB),¹³ surface-enhanced Raman spectroscopy (SERS),¹⁴ computational algorithms,¹⁵ as well as spatially offset Raman spectroscopy.¹⁶ However, it remains difficult to obtain Raman signals with sufficient quality in a noninvasive manner for fragile solid samples in the presence of severe fluorescence.^{3,17,18} Non-contact measurement, low laser power, and easy operation without sample pollution and damage are urgent needs for vulnerable samples but extremely challenging in the existing methods.

SERS is utilized for effective identification of Raman signals with enhancement of Raman peaks and quenching of fluorescence.^{1,19} The electromagnetic enhancement mechanism (EM) and the chemical enhancement mechanism (CM) are the fundamental mechanisms underlying SERS effects. SERS can also quench fluorescence by the Förster resonance

energy transfer (FRET) effect.²⁰ Nevertheless, EM and FRET are highly localized on the nanometer scale near the substrate. Meanwhile, CM is based on charge transfer (CT),^{1,19,21} which is a ubiquitous and essential process in nature.^{22–24} At present, CT also relies on coinage-metal and several nonmetal substrates.^{25–28} Therefore, the method of long-distance CT without enhancement substrates may be a potential way to detect fluorescent but vulnerable samples.

It was reported that an ion flux can influence the nonlinear Raman light emission because extra electrons were transferred from negatively ionized air molecules to the sample surface.²⁹ As a kind of ion flux, ionic wind (IW) is a flow of cold plasma composed of mobile charged and neutral gas molecules as well as electrons.^{30,31} It has been applied in the fields of thermal engineering and satellite propulsion³² and can be generated by polarized needle-net (Figure 1a) or needle-plate electrodes.^{33–35} The charged ion particles in IW can be delivered

Received: September 22, 2022

Accepted: December 19, 2022

Published: December 28, 2022



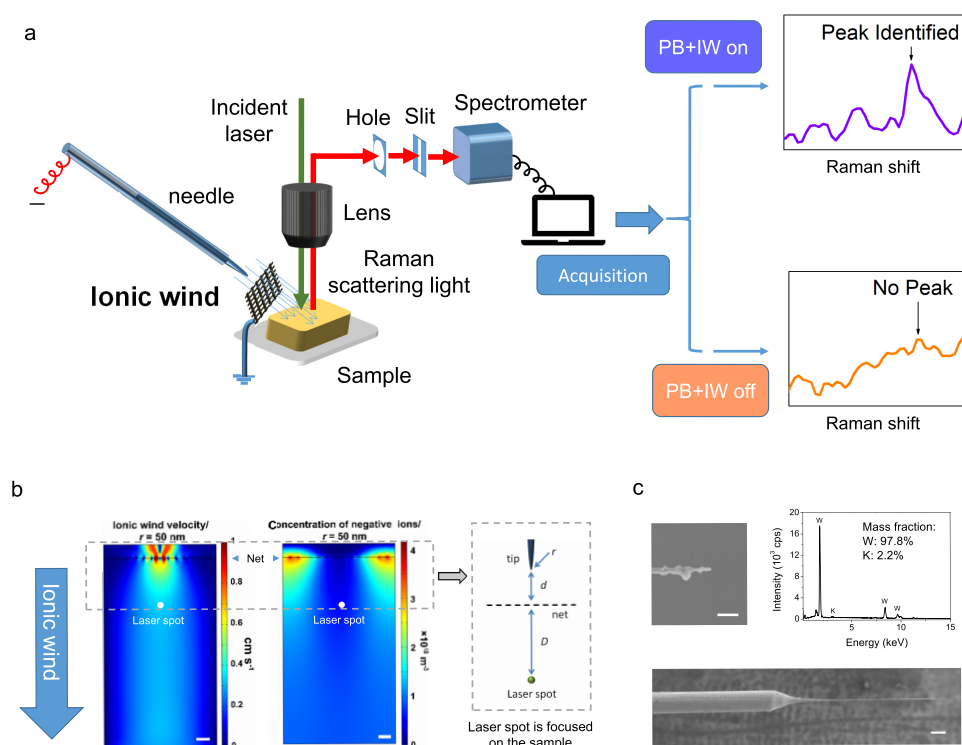


Figure 1. Experimental setup and FDTD simulations for the needle-net setup. (a) Schematic of the needle-net electrodes, which generate IW (the sample is placed around 3 mm behind the net). (b) FDTD results of the needle-net setup, indicating the distribution of the ionic wind velocity (unit: cm/s) and concentration of negative ions (unit: m^{-3}) with r of 50 nm. r : the radius curvature of the tip, d : the distance between the tip and the net. D : the distance between the net and the laser spot on the sample. In panel (b), d is 0.4 mm, the voltage (U) is -300 V , and the scale bar is 1 mm. (c) SEM images and EDS result (upper right) of the needle with r of 50 nm: the apex (upper left, scale bar: $1 \mu\text{m}$), the whole view (bottom, scale bar: $200 \mu\text{m}$), and the EDS result (upper right). IW: ionic wind. FDTD: finite-difference time-domain. EDS: energy dispersive spectroscopy.

and transferred to targeted samples over a distance of several millimeters, so that it can be regarded as a remote and tunable ionization source for CT. Herein, for the first time, we propose a method of ionic-wind-enhanced Raman spectroscopy (IWERS) incorporated with PB to perform substrate-free Raman measurements of several fragile samples by means of CT at a macroscopic distance. We aim at proving whether IWERS is capable of enhancing Raman peaks and suppressing fluorescence simultaneously in the noncontact mode when the samples are positioned behind the net. The synergistic effect of IW and PB will be investigated. Density functional theory (DFT) calculations will be employed to demonstrate the possible mechanisms of IWERS. Then, nondestructive examinations of an ancient brick, dyed textiles, a piece of amber, and a red rock as an analogue to Mars geological samples will be performed to verify the feasibility of IWERS by searching for weak Raman peaks under the strong fluorescence background.

RESULTS AND DISCUSSION

Enhancement of Raman Signals of Nonfluorescent Materials by IWERS. The nonfluorescent materials sodium carbonate (Na_2CO_3) and hexadecyl trimethyl ammonium bromide (CTAB) were used to examine the effect of IWERS on Raman enhancement (see Figure 2a–d and Supporting Information S3 and S4). At a U of -300 V and an r of 50 nm, the highest enhancement ratio (P_e) of the Raman peak of Na_2CO_3 at 1083 cm^{-1} was $21.6\% \pm 12.0\%$ at a duration time (t) of 20 min, which was significantly higher than P_e of $3.7\% \pm 3.3\%$ at t of 0 min ($p < 0.05$). P_e first increased and then

decreased. Under the same conditions, the main Raman peak of CTAB at 2883 cm^{-1} yielded the highest P_e of $18.6\% \pm 4.4\%$ at a t of 20 min, which was also significantly higher than P_e of $6.1\% \pm 5.0\%$ at t of 0 min ($p < 0.05$). The r of 50 nm was selected because the concentration of negative ionic particles is much higher than that of $2 \mu\text{m}$ behind the net. Therefore, both organic and inorganic compounds can be enhanced by IW.

In SERS, CT can change the electronic structure of the analyte molecules. The enhancement factor of the CM is usually 10^1 – 10^2 -fold.^{19,36} When the plasma flows close to the sample surface, an electrostatic sheath emerges (the thickness of this sheath is on the order of $1 \mu\text{m}$ for an r of 50 nm at room temperature), and the charged particles are absorbed by the sample.³⁷ Because the concentration of negatively ionic particles is on the order of 10^{18} m^{-3} (-300 V , 50 nm tip; see Figure 1b) and is much higher than that of electrons (on the order of 10^8 m^{-3} , see Figure S3), charged particles play a dominant role in CT. In IWERS, these adsorbed ions interact with sample molecules by means of dipole–ion interactions or dispersion forces (Figure 2e).³⁸ The surface molecules of the sample possess a much larger Raman scattering cross section than the internal molecules, so the surface molecules contribute most to the Raman signal enhancement.^{39,40}

To confirm the effect of CT for IWERS, an air flow (AF) test was performed with a small pump blowing air to CTAB with a similar velocity of IW behind the net. In this case, a Raman enhancement of $2.7\% \pm 1.0\%$ was observed ($n = 3$), which might be due to the presence of natural negatively ionic particles in air.⁴¹ Another test for Na_2CO_3 under PB + IW yielded an enhancement ratio similar to that of IW only (see

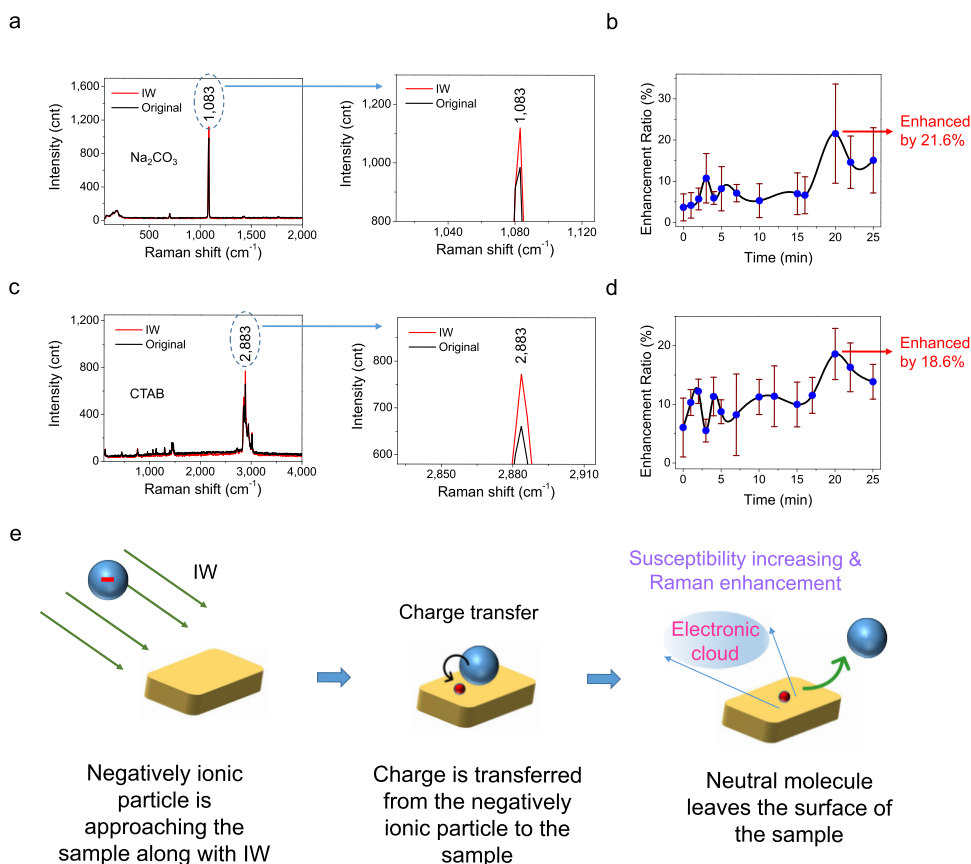


Figure 2. IWERS of nonfluorescent materials. (a,b) Enhanced Raman spectra of Na_2CO_3 under IW only: the original and representative enhanced Raman spectra (a) and the trend of the enhancement ratio of the Raman peak at 1083 cm^{-1} over time (the highest ratio: $21.6\% \pm 12.0\%$, $n = 3$) (b). (c,d) Enhanced Raman spectra of CTAB under IW only: the original and representative enhanced Raman spectra (c) and the trend of the enhancement ratio of the Raman peak at 2883 cm^{-1} over time (the highest ratio: $18.6\% \pm 4.4\%$, $n = 3$) (d). In (a)–(d), U is -300 V , r is 50 nm , the net is 40 mesh, and d is 0.4 mm . (e) Illustration of interactions between the sample and the ionic particles in IW.

Figure 2a and S10). These results confirm that PB is not able to enhance the Raman peaks and AF only has a weak enhancement effect, indicating that the observed enhancement is attributed to IW.

IWERS for glycine was also performed. DFT calculations suggested that electronic doping can supply free electrons to the valence band of glycine (see Supporting Information S7), continuously increasing its relative susceptibility from 2.5 without electronic doping to 3.3 with $0.22\text{ e}/\text{unit-cell}$ doping. These results are consistent with the experimental results (Figures S11 and S12).

Detection of Fluorescent Samples by Incorporation of IW with PB. PB has been known as a routine method to alleviate fluorescence interference. To demonstrate the effects of IWERS coupled with PB on fluorescent materials, graphitic carbon nitride (g-CN), which is a two-dimensional (2D) optoelectronic semiconductor⁴² and shows intrinsic strong fluorescence and thermal stability,^{43,44} was prepared and analyzed (see Supporting Information S3 and S11). The ratio of fluorescence quenching (K) is defined as the integral area of the quenched spectrum divided by that of the original spectrum (see Supporting Information S11) as a function of t . Therefore, a larger K indicates a more significant fluorescence quenching performance. In Figures 3a and 4b, K is $3.2\% \pm 1.8\%$ for IW only at a t of 20 min, indicating that IW slightly quenches fluorescence. IWERS is able to quench fluorescence due to oxygen (O_2) in air, which is a typical fluorescence

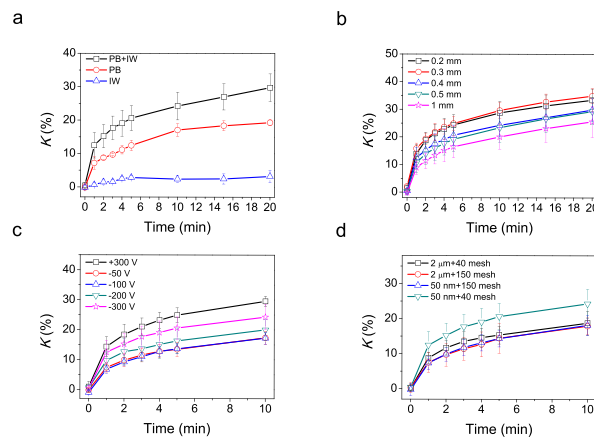


Figure 3. Variation in the fluorescence quenching ratio (K) with different conditions for the needle-net setup ($n = 5$) and typical Raman spectra of g-CN. (a) Different configurations. (b) Electrode distance. (c) Voltage. (d) Combination of the curvature radius of the tip apex and the mesh of the net. The configuration of PB + IW, U of -300 V , r of 50 nm , d of 0.4 mm , and the net of 40 mesh are selected as the optimized combination.

quencher.^{10,45} Interestingly, the sum of K for IW only ($3.2\% \pm 1.8\%$) and PB only ($19.3\% \pm 0.9\%$) is much lower than that of PB + IW ($29.8\% \pm 0.04\%$), which implies a synergism of fluorescence quenching by IW and PB. Thus, IWERS

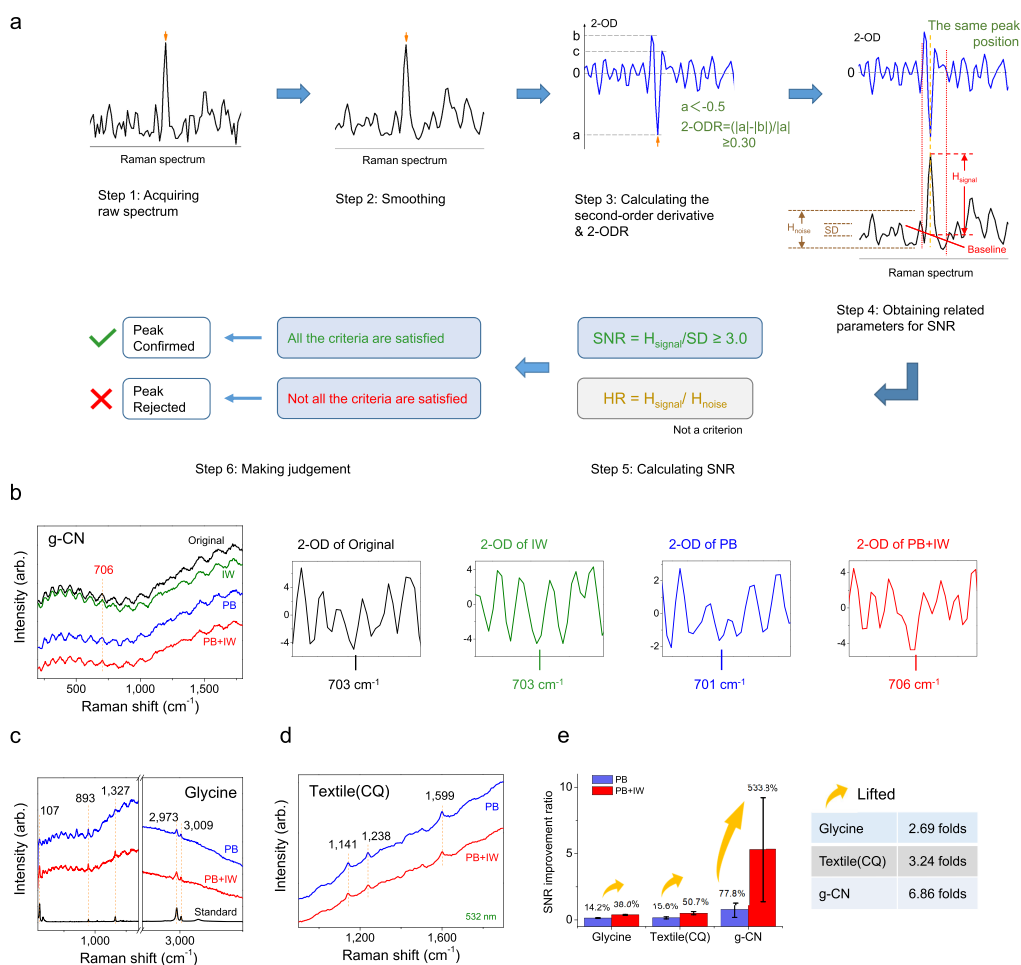


Figure 4. Protocol for the identification of a Raman peak and improvement of the SNR. (a) Flow chart that illustrates the criterion including four rules for identifying a Raman peak. (b) Typical Raman spectra of g-CN and the variation of the 2-OD. The Raman peak at 706 cm⁻¹ was observed with PB + IW. The four smaller panels on the right show the change of the 2-OD for varied conditions. (c) Typical Raman spectra of glycine mixed with g-CN (pure glycine shows no fluorescence, and its spectrum is shown as standard). (d) Typical Raman spectra of textile (CQ) [a piece of cotton that was colored by Cuqian (CQ), a plant dye made from thick *Rubia cordifolia* Linn.]. (e) SNR improvement ratio of PB and PB + IW for glycine mixed with g-CN, textile (CQ), and g-CN, respectively ($n = 3$). In (b)–(d), the needle-net electrodes were utilized ($r = 50$ nm and $U = -300$ V), and the laser wavelength is 532 nm. PB: photobleaching, EF: electric field, IW: ionic wind, 2-ODR: the second-order derivative ratio, SNR: signal-to-noise ratio, HR: signal-to-noise height ratio, and arb.: arbitrary unit.

incorporated with PB is more effective to quench fluorescence. The optimization of U , r , d , and net mesh was further investigated (Figure 3b–d). The 50 nm tip accompanied by the 40-mesh net was determined to be the standard configuration. Although the K value at a U of +300 V was $29.6\% \pm 1.6\%$ higher than $24.3\% \pm 4.1\%$ at -300 V ($t = 10$ min), there were no peaks observed at +300 V. In addition, there was no difference in K between the sample–net distances of 0.3 cm ($24.3\% \pm 4.1\%$) and 1.1 cm ($24.8\% \pm 3.4\%$) ($t = 10$ min), confirming that the flow field behind the net was approximately uniform and that the sample did not require precise positioning behind the net.

Considering weak signals, a criterion for identifying Raman peaks was proposed. A candidate Raman peak should be satisfied with the four rules: (a) the absolute value of the minimum second-order derivative (2-OD) should be less than -0.5 ; (b) the ratio of the second-order derivative (2-ODR) should be equal to or larger than 0.30; (c) the signal-to-noise ratio (SNR) should be equal to or larger than 3.0; and (d) the peak positions of the 2-OD and raw Raman spectra should be the same. Only when all the above four rules are satisfied, a

candidate peak can be identified (see Figure 4a and Supporting Information S8 and S11 for the calculation flow and details). For instance, there are four main Raman peaks for g-CN at 706 and 477 cm⁻¹ (layer–layer deformation vibrations⁴³), 980 cm⁻¹ (symmetric ring breathing mode⁴⁴), and 1238 cm⁻¹ (N=C (sp²) bending vibration⁴³). The candidate peak locates at 706 cm⁻¹. Clearly, the 2-OD of this peak changed dramatically (Figure 4b). Since no peaks attributed to g-CN were observed in the original spectrum (see Figure 4b and Table S1), Raman enhancement could not be observed directly. DFT calculations were employed to determine the Raman enhancement of g-CN and show that the relative susceptibility increased approximately linearly by electronic doping of charged particles in IW to the sample (from 3.41 without electrons to 3.76 with 0.22 e/unit-cell), thus confirming the enhancement of the Raman peaks (see Supporting Information S7).

Therefore, with the optimized conditions, the major peak of g-CN at 706 cm⁻¹ was observed by PB + IW under a strong fluorescence background, which shows that IWERS incorporated with PB has the capacity to detect strongly fluorescent

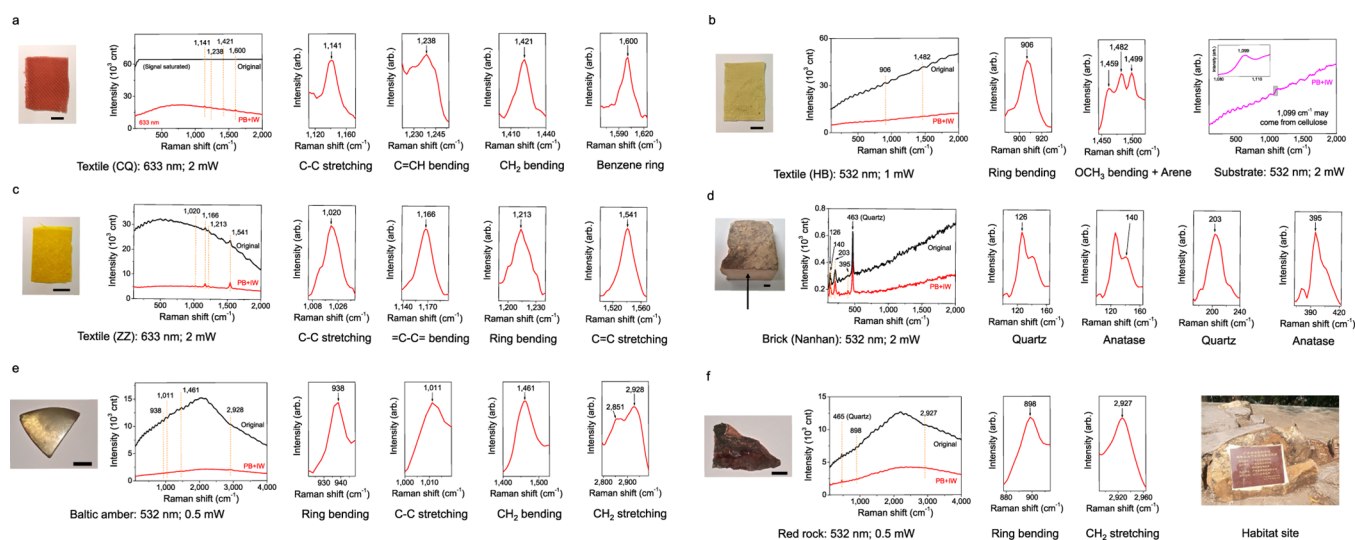


Figure 5. Raman spectra of several real-world samples with PB + IW. (a) Raman spectra of textile (CQ) [a piece of cotton that was colored by Cuqian (CQ), a plant dye made from thick *Rubia cordifolia* Linn.]. Both the 532 nm (shown in Figure 4d) and 633 nm (this figure) lasers were applied that worked well. (b) Raman spectra of textile (HB) [a piece of cotton that was colored by Huangbo (HB), a plant dye made from *Phellodendron amurense* Rupr.]. When the laser power increases, the substrate (cellulose) peak emerges, which shows that the fastness is low. (c) Raman spectra of textile (ZZ) [a piece of silk that was colored by Zhizi (ZZ), a plant dye made from *Gardenia jasminoides* Ellis]. (d) Raman spectra of the ancient brick made in the Nanhan Dynasty located in South China more than 1000 years ago. TiO_2 (anatase) was identified that can be used as a white pigment. The arrow indicates the brick body that was tested. (e) Raman spectra of a piece of Baltic amber. The peak at 1461 cm^{-1} is correlated with amber's maturity. (f) Raman spectra of the red rock collected from the top of the hill near the campus of the South China University of Technology. Organics were found on this "sterile" rock that is mimicking Mars geological samples. All the scale bars are 0.5 cm. arb.: arbitrary unit.

samples. The other peaks did not emerge. Besides, from Figure 4b, we can see that the average SNR of the four theoretical peaks can be improved via PB only and PB + IW by $77.8\% \pm 58.8\%$ and $533.8\% \pm 387.8\%$, respectively ($p = 0.057$). The SNR improvement ratio of PB + IW to PB only is thus 6.86-fold for g-CN (Figure 4e), while it is 2.69-fold ($p < 0.05$) for glycine mixed with g-CN (see Figure 4c,e for Raman spectra and comparison, and see Tables S1 and S2 for the representative SNR value of every peak of g-CN and glycine mixed with g-CN, respectively). This shows that PB + IW is much better than solely applying PB, the common method, for fluorescent samples.

Examination of the Real-World Samples. We further applied this approach to examine several real samples with strong fluorescence interference, including dyed textiles, an ancient brick, a piece of amber, and a natural red rock (see Figure 5, and Supporting Information S9–S11). This non-invasive needle-net setup was employed for Raman detections under the optimized parameters mentioned above, and some key Raman peaks were observed. First, three types of colored textiles, which were made by the National Museum of China with the dyeing procedures totally following the ancient ones, were examined (see Methods). A red piece of cotton was colored by Cuqian (CQ), a dye made from thick *Rubia cordifolia* Linn. and thus called textile (CQ) (Figure 5a). The sample has strong fluorescence, and the peak at 1600 cm^{-1} shows that it has a benzene-ring structure. PB only and PB + IW tests were also applied for textile (CQ) (Figure 4d). The SNR is improved by $15.6\% \pm 7.9\%$ and $50.7\% \pm 11.8\%$, respectively ($p < 0.05$), and the SNR improvement ratio is 3.24-fold, which is on the same order of g-CN and glycine mixed with g-CN (Figure 4e). All these results suggested that regardless of the origin and components of samples, the improvement ratio of the SNR can be significantly enhanced

by about 3-fold under PB + IW compared to PB only. This is vitally important for Raman peaks with an SNR between 1 and 2, which are invisible by common Raman spectroscopy and can be successfully recovered by our apparatus attributed to the much improvement of the SNR.

The other two textiles were examined next. A yellow piece of cotton was colored by Huangbo (HB), a dye made from *Phellodendron amurense* Rupr. The Raman spectra of textile (HB) are shown in Figure 5b. The peak at 906 cm^{-1} and the peak group at 1482 cm^{-1} show that the dye has a condensed-ring-arene structure. When the power of the 532 nm laser increases from 1 to 2 mW, the peaks of the dye disappear, and the peak at 1099 cm^{-1} emerges, which reveals that the substrate of the sample may be composed of cellulose and the color fastness is low since 2 mW power is able to totally penetrate the dye layer. A yellow piece of silk was colored by Zhizi (ZZ), a dye made from *Gardenia jasminoides* Ellis. The Raman spectra of textile (ZZ) are shown in Figure 5c. The three dyes possess distinguished Raman peaks, respectively, which are characteristic of every textile. A dramatically improved SNR was attributed to the identification of these peaks.

Next, an ancient brick made in the Nanhan Dynasty (AD 917–971, located in South China) was analyzed (Figure 5d). This relic is made of sintered clay with a white body and a black surface. Apart from the peak at 140 cm^{-1} , the weak peak at 395 cm^{-1} of TiO_2 (anatase) was clearly observed via PB + IW with an SNR higher than 5, which was unseen in the original spectrum. Therefore, anatase was successfully confirmed by both of the peaks at 140 and 395 cm^{-1} . Therefore, we can speculate that the white color is mainly attributed to anatase. Furthermore, for a piece of Baltic amber (see Figure

Se and Supporting Information S11), K was $81.5\% \pm 2.8\%$ using PB + IW ($n = 3$). Vibrational modes at 938 cm^{-1} (ring bending), 1011 cm^{-1} (C–C stretching), 1461 cm^{-1} (CH_2 bending), and 2928 cm^{-1} (CH_2 stretching) were observed. The peak observed at 1461 cm^{-1} can be correlated with amber's maturity.⁴⁶

Finally, a red rock with no observable plants was examined, which can be regarded as an analogue to Mars rock samples (see Figure Sf and Supporting Information S11). The background interference was suppressed efficiently since K is equal to $54.6\% \pm 9.0\%$ ($n = 3$), and the peaks at 898 and 2927 cm^{-1} were discernible from the background, which were assigned to ring bending and CH_2 stretching, respectively. The two peaks are indicative of organic molecules, and scientists are now eager to find them on Mars. Mars is a red but sterile planet. Seeking for life is just the main task for the US Mars rover *Perseverance*, which is equipped with Raman spectrometers first time in the world. It also carries an auxiliary helicopter for image navigation.^{17,18,47} We are thus inspired to an aircraft that is able to fly and simultaneously acquire Raman signals on Mars. This aerial vehicle can be propelled by the thrust of IW⁴⁸ or magnetohydrodynamics⁴⁹ and is able to record clear Raman signals by IWERS.

CONCLUSIONS

In this study, IWERS incorporated with PB was first proposed and proved to effectively improve the SNR of Raman peaks by enhancing Raman signals and quenching fluorescence in a noninvasive and substrate-free way. IW induces long-range CT to the sample surface on the millimeter scale, which plays a vital role in Raman enhancement (see Table S3 in Supporting Information for a summary of the different roles of the main species). In traditional enhancement methods like SERS, CT only occurs within a distance of several nanometers between the substrate and sample, so that close contact between them is required. On the contrary, the IWERS method is able to transfer charges on the macroscopic scale, and the physical contact is thus no longer needed. PB is a common method to suppress fluorescence but shows a much lower SNR enhancement ratio than IWERS incorporated with it. IWERS shows the capacity to discover weak Raman peaks under the fluorescence background.

Although the enhancement ratio is lower in IWERS than the common methods such as SERS, IWERS presents a unique ability to address the fluorescence interference problem for fragile samples in the real world. It can be considered as a new option for the Raman toolbox. Considering that CM can enhance Raman peaks by 10^1 – 10^2 -fold, a higher enhancement ratio may be achieved by IWERS if more ion particles are generated and propelled to the sample. As the dominant factors of IW, the applied voltage U and r of the tip can be further optimized to obtain a higher concentration of negatively ionic particles, which is still far below a safe limit for the sample surface.⁵⁰ Therefore, more Raman peaks might be recovered. The examinations of three sorts of the real-world samples, including textiles, minerals, and jewelries, suggest the promising application of IWERS in acquiring pure Raman spectroscopy in the presence of severe fluorescence. As a result, IWERS can be expected to be a routine experimental approach for Raman spectroscopy, either in lab or in outer space.

EXPERIMENTAL SECTION

Experimental Setup for IWERS. In this study, a needle-net setup was utilized. Such a setup does not require contact of the sample, thus preventing sample contamination and destruction (Figure 1a). The tip curvature radii (r) of the needles were 50 nm. All the needles were composed of tungsten (see Methods, Figure 1c and S1), and a static polarization voltage (U) was applied to establish a stable flow field. The finite-difference time-domain (FDTD) method (see Supporting Information S11) was used to simulate the IW velocity and concentration of the negatively ionic particles (see Figure 1b and S2), as well as the strength of the electric field (EF), spatial density of positively ionic particles and electrons, as well as net charges (Figure S3). The EF at the tip apex was on the order of 10^6 V/m , and a uniform flow field appeared from 0.3 to 1.5 cm behind the net, while the IW velocity was approximately 0.5 cm/s at U of -300 V and r of 50 nm. Higher U and smaller r can lead to higher EF. In all the experiments, a 532 or 633 nm continuous wave (cw) laser with a laser power at the sample no greater than 2 mW was employed (see Supporting Information S1 for details).

Parameters of Raman Spectroscopy. A LabRAM Aramis Raman spectrometer (HORIBA Jobin-Yvon (HJY)) was utilized in this experiment. The wavelength of the cw laser was 532 or 633 nm for all the experiments. The laser power for the needle-net setup was not higher than 2 mW at the sample. For the g-CN sample, the time of accumulation was 1 s twice because a longer integral time would make the charge-coupled device signal saturated for strong fluorescence and prevent an accurate peak area from being calculated. As a narrower slit can improve the SNR, the slit was set to $100\text{ }\mu\text{m}$, and the hole was set to $400\text{ }\mu\text{m}$. The grating was 600 gr/mm, so the average spectral resolution was 4 cm^{-1} . The lens was a 50 \times LMPlan with a long working distance (Olympus; the numerical aperture was 0.50). The diameter of the laser spot was $2\text{ }\mu\text{m}$. The door of the instrument was closed during the experiments to eliminate surrounding interferences. The environment of the laboratory was stable during the experiments [temperature: $(24.5 \pm 0.5)\text{ }^\circ\text{C}$, humidity: $(50 \pm 1)\%$, and atmospheric pressure: $(1004 \pm 4)\text{ hPa}$].

Electrode Setup. For both the needle-net and needle-plate setup (Figure S14), a screw gauge platform (Runjia Pneumatic Technology) was utilized to control the distance between the needle and the net/plate, with a precision of $\pm 20\text{ }\mu\text{m}$. In the needle-net setup, the needle was clamped by a metal clip that was welded to an iron rod. The rod was connected to the platform by means of a strong neodymium magnet. The net was made of stainless steel with dimensions of $9\text{ mm} \times 9\text{ mm}$ and was linked to the ground. One net was 40 mesh (wire diameter: 0.13 mm, hole: 0.52 mm), and the other net was 150 mesh (wire diameter: 0.06 mm, hole: 0.11 mm). The net was connected with a copper (Cu) wire to a magnet that also attracted an iron rod and could rotate freely so that the angle of the net could be adjusted. The samples were placed behind the net (the angle between the direction of the IW velocity and the normal of the sample surface was approximately 45°). A U value of -300 V and a d of 0.4 mm were selected when the other parameters were examined. In the needle-plate setup, the needle was fastened to a Cu sheet that was also fixed to the microscope's stage and linked with the power supply. The plate that was linked to the ground was made of Cu with dimensions of $10\text{ mm} \times 8\text{ mm}$ and connected to the platform by a strong

neodymium magnet. The g-CN powder was adsorbed on the tip of the needle. A U value of -300 V and a d of 0.2 mm were selected when the other parameters were examined. Parallel tests for the needle-net and needle-plate setup were repeated five and three times, respectively. Under all the working conditions, the increase in the air temperature near the facility was less than 4 °C, so the heat effect could be omitted. To verify the effects of charged ions and oxygen molecules in IWERS for the needle-net setup, a test with pure AF instead of IW was performed. For comparison, a small air pump (LXHE Inc., LX-JY0300; 2.5 W) was used to generate AF that was directed to the surface of the sample by a plastic tube. The input voltage of the pump was adjusted to give a comparable outlet velocity of AF with IW.

■ ASSOCIATED CONTENT

SI Supporting Information

The Supporting Information is available free of charge at <https://pubs.acs.org/doi/10.1021/acs.analchem.2c04189>.

Discussion of Raman acquisition in the presence of fluorescence, the needle characterization and FDTD results in the needle-net setup, the characterization of the materials, further IWERS experiments, the parallel-plate electrode setup, the needle-plate electrode setup, DFT calculations, the explanation of the criterion for identifying Raman peaks, characterization of the real-world samples, calculation of Raman spectra for the real-world samples, and additional methods (PDF)

■ AUTHOR INFORMATION

Corresponding Authors

Qingyou Liang – Analytical and Testing Center and School of Material Science and Engineering, South China University of Technology, Guangzhou 510640, China; orcid.org/0000-0002-4213-1792; Email: liangqy@scut.edu.cn

Xiangjun Gong – School of Material Science and Engineering, South China University of Technology, Guangzhou 510640, China; orcid.org/0000-0001-7049-944X; Email: msxjgong@scut.edu.cn

Xianfeng Yang – Analytical and Testing Center, South China University of Technology, Guangzhou 510640, China; Email: czxfyang@scut.edu.cn

Chunlin Deng – School of Material Science and Engineering, South China University of Technology, Guangzhou 510640, China; Email: chldeng@scut.edu.cn

Shi Liu – School of Science, Westlake University, Hangzhou 310024, China; Institute of Natural Sciences, Westlake Institute for Advanced Study, Hangzhou 310024, China; orcid.org/0000-0002-8488-4848; Email: liushi@westlake.edu.cn

Authors

Jinchao Liu – Analytical and Testing Center and School of Chemistry and Chemical Engineering, South China University of Technology, Guangzhou 510640, China

Changming Ke – School of Science, Westlake University, Hangzhou 310024, China; Institute of Natural Sciences, Westlake Institute for Advanced Study, Hangzhou 310024, China

Jie Dong – Department of Radiation Oncology, The Third Affiliated Hospital of Sun Yat-sen University, Guangzhou 510630, China

Guosheng Song – Analytical and Testing Center, South China University of Technology, Guangzhou 510640, China

Pu Feng – School of Material Science and Engineering, South China University of Technology, Guangzhou 510640, China

Huakang Yu – School of Physics, South China University of Technology, Guangzhou 510640, China

Jie Cui – Analytical and Testing Center, South China University of Technology, Guangzhou 510640, China

Zhiyuan Li – School of Physics, South China University of Technology, Guangzhou 510640, China

Guangzhao Zhang – School of Material Science and Engineering, South China University of Technology, Guangzhou 510640, China; orcid.org/0000-0002-0219-3729

Complete contact information is available at:

<https://pubs.acs.org/10.1021/acs.analchem.2c04189>

Author Contributions

G.Z.Z. and Q.Y.L. conceived the project. Q.Y.L., X.F.Y., and X.J.G. designed the experiments and fabricated the device. Q.Y.L. and G.S.S. collected and analyzed the data with J.C.L.'s help. J.C., J.C.L., and X.F.Y. prepared and characterized the tungsten needles. C.L.D. and Q.Y.L. prepared and characterized the tested materials. S.L., Z.Y.L., C.M.K., and H.K.Y. conducted the theoretical analysis. S.L. and C.M.K. conducted the DFT calculations. J.D. performed signal processing analysis and radiation monitoring. X.J.G., H.K.Y., and P.F. conducted the COMSOL simulations. Q.Y.L. collected the rock sample. X.J.G. collected the brick sample. Q.Y.L. proposed the criterion for peak identification. Q.Y.L., X.J.G., and X.F.Y. wrote the manuscript with input from all authors.

Notes

The authors declare no competing financial interest.

■ ACKNOWLEDGMENTS

We thank X. H. Xiang for the discussions on the manuscript writing. We also thank Y. Y. Wei, A. D. Wang, M. Wan, S. J. Huang, and J. Ren for help in characterizing the materials. We thank S. W. Yue for providing and identifying the amber sample. We thank M. J. Zhang and X. L. Li for help with the FDTD simulations. We thank S. D. Jiang for beneficial discussions on quantum mechanics. We also thank X. L. Cheng for providing colored textiles. This research was supported by the National Natural Science Foundation of China (grant nos. 21973032, 21637001, 52172142, 51972120, 51801065, and 51772105), the Science and Technology Projects in Guangzhou (grant no. 202201010705), the Fundamental Research Funds for the Central Universities (grant nos. 2019ZD02 and 2022ZYGXZR106), the Fund of the Key Laboratory of Luminescence from Molecular Aggregates of Guangdong Province (grant no. 2019B030301003), and the Guangdong Provincial Young Innovative Talents Program (grant no. 2020KQNCX002).

■ REFERENCES

- (1) Li, J. F.; Huang, Y. F.; Ding, Y.; Yang, Z. L.; Li, S. B.; Zhou, X. S.; Fan, F. R.; Zhang, W.; Zhou, Z. Y.; Wu, D. Y.; Ren, B.; Wang, Z. L.; Tian, Z. Q. *Nature* **2010**, *464*, 392–395.
- (2) Hanke, F.; Mooij, B. J. A.; Ariese, F.; Böttger, U. *J. Raman Spectrosc.* **2019**, *50*, 969–982.
- (3) Ziemann, M. A.; Madariaga, J. M. *J. Raman Spectrosc.* **2021**, *52*, 8–14.

- (4) Gauffrès, E.; Tang, N. Y.-W.; Lapointe, F.; Cabana, J.; Nadon, M.-A.; Cottenye, N.; Raymond, F.; Szkopek, T.; Martel, R. *Nat. Photonics* **2014**, *8*, 72–78.
- (5) Kagan, M. R.; McCreery, R. L. *Anal. Chem.* **1994**, *66*, 4159–4165.
- (6) Moore, J. E.; Fraas, L. M. *Anal. Chem.* **1973**, *45*, 2009–2014.
- (7) Ding, S. Y.; Yi, J.; Li, J. F.; Ren, B.; Wu, D. Y.; Panneerselvam, R.; Tian, Z. Q. *Nat. Rev. Mater.* **2016**, *1*, 16021.
- (8) Wei, D.; Chen, S.; Liu, Q. *Appl. Spectrosc. Rev.* **2015**, *50*, 387–406.
- (9) Morton, S. M.; Jensen, L. J. *Am. Chem. Soc.* **2009**, *131*, 4090–4098.
- (10) Lin, C. W.; Bachilo, S. M.; Weisman, R. B. *J. Am. Chem. Soc.* **2020**, *142*, 21189–21196.
- (11) Henderson, J. N.; Ai, H. W.; Campbell, R. E.; Remington, S. J. *Proc. Natl. Acad. Sci. U. S. A.* **2007**, *104*, 6672–6677.
- (12) Guo, S. X.; Chernavskaia, O.; Popp, J.; Bocklitz, T. *Talanta* **2018**, *186*, 372–380.
- (13) Dutta, S. B.; Krishna, H.; Khan, K. M.; Gupta, S.; Majumder, S. K. *Spectrochim. Acta, Part A* **2021**, *247*, No. 119144.
- (14) Walters, C. M.; Pao, C.; Gagnon, B. P.; Zamecnik, C. R.; Walker, G. C. *Adv. Mater.* **2018**, *30*, No. 1705381.
- (15) Chen, S.; Kong, L. M.; Xu, W. B.; Cui, X. Y.; Liu, Q. *IEEE Access* **2018**, *6*, 67709–67717.
- (16) Conti, C.; Botteon, A.; Colombo, C.; Realini, M.; Matousek, P. *Analyst* **2016**, *141*, 5374–5381.
- (17) Bhartia, R.; Beegle, L. W.; DeFlores, L.; Abbey, W.; Hollis, J. R.; Uckert, K.; Monacelli, B.; Edgett, K. S.; Kennedy, M. R.; Sylvia, M.; Aldrich, D.; Anderson, M.; Asher, S. A.; Bailey, Z.; Boyd, K.; Burton, A. S.; Caffrey, M.; Calaway, M. J.; Calvet, R.; Cameron, B.; Caplinger, M. A.; Carrier, B. L.; Chen, N.; Chen, A.; Clark, M. J.; Clegg, S.; Conrad, P. G.; Cooper, M.; Davis, K. N.; Ehlmann, B.; Facto, L.; Fries, M. D.; Garrison, D. H.; Gasway, D.; Ghaemi, F. T.; Graff, T. G.; Hand, K. P.; Harris, C.; Hein, J. D.; Heinz, N.; Herzog, H.; Hochberg, E.; Houck, A.; Hug, W. F.; Jensen, E. H.; Kah, L. C.; Kennedy, J.; Krylo, R.; Lam, J.; Lindeman, M.; McGlown, J.; Michel, J.; Miller, E.; Mills, Z.; Minitti, M. E.; Mok, F.; Moore, J.; Nealson, K. H.; Nelson, A.; Newell, R.; Nixon, B. E.; Nordman, D. A.; Nuding, D.; Orellana, S.; Pauken, M.; Peterson, G.; Pollock, R.; Quinn, H.; Quinto, C.; Ravine, M. A.; Reid, R. D.; Riendeau, J.; Ross, A. J.; Sackos, J.; Schaffner, J. A.; Schwochert, M.; Shelton, M. O.; Simon, R.; Smith, C. L.; Sobron, P.; Steadman, K.; Steele, A.; Thiessen, D.; Tran, V. D.; Tsai, T.; Tuite, M.; Tung, E.; Wehbe, R.; Weinberg, R.; Weiner, R. H.; Wiens, R. C.; Williford, K.; Wollonciej, C.; Wu, Y. H.; Yingst, R. A.; Zan, J. *Space Sci. Rev.* **2021**, *217*, 58.
- (18) Wiens, R. C.; Maurice, S.; Robinson, S. H.; Nelson, A. E.; Cais, P.; Bernardi, P.; Newell, R. T.; Clegg, S.; Sharma, S. K.; Storms, S.; Deming, J.; Beckman, D.; Ollila, A. M.; Gasnault, O.; Anderson, R. B.; Andre, Y.; Michael Angel, S.; Arana, G.; Auden, E.; Beck, P.; Becker, J.; Benzerara, K.; Bernard, S.; Beyssac, O.; Borges, L.; Bousquet, B.; Boyd, K.; Caffrey, M.; Carlson, J.; Castro, K.; Celis, J.; Chide, B.; Clark, K.; Cloutis, E.; Cordoba, E. C.; Cousin, A.; Dale, M.; Deflores, L.; Delapp, D.; Deleuze, M.; Dirmyer, M.; Donny, C.; Dromart, G.; George Duran, M.; Egan, M.; Ervin, J.; Fabre, C.; Fau, A.; Fischer, W.; Forni, O.; Fouchet, T.; Fresquez, R.; Frydenvang, J.; Gasway, D.; Gontijo, I.; Grotzinger, J.; Jacob, X.; Jacquino, S.; Johnson, J. R.; Klisiewicz, R. A.; Lake, J.; Lanza, N.; Laserna, J.; Lasue, J.; Le Mouelic, S.; Leggett, C.; Leveille, R.; Lewin, E.; Lopez-Reyes, G.; Lorenz, R.; Lorigny, E.; Love, S. P.; Lucero, B.; Madariaga, J. M.; Madsen, M.; Madsen, S.; Mangold, N.; Manrique, J. A.; Martinez, J. P.; Martinez-Frias, J.; McCabe, K. P.; McConnochie, T. H.; McGlown, J. M.; McLennan, S. M.; Melikechi, N.; Meslin, P. Y.; Michel, J. M.; Mimoun, D.; Misra, A.; Montagnac, G.; Montmessin, F.; Mousset, V.; Murdoch, N.; Newsom, H.; Ott, L. A.; Ousnamer, Z. R.; Pares, L.; Parot, Y.; Pawluczyk, R.; Glen Peterson, C.; Pilleri, P.; Pinet, P.; Pont, G.; Poulet, F.; Provost, C.; Quertier, B.; Quinn, H.; Rapin, W.; Reess, J. M.; Regan, A. H.; Reyes-Newell, A. L.; Romano, P. J.; Royer, C.; Rull, F.; Sandoval, B.; Sarrao, J. H.; Sautter, V.; Schoppers, M. J.; Schroder, S.; Seitz, D.; Shepherd, T.; Sobron, P.; Dubois, B.; Sridhar, V.; Toplis, M. J.; Torre-Fdez, I.; Trettel, I. A.; Underwood, M.; Valdez, A.; Valdez, J.; Venhaus, D.; Willis, P. *Space Sci. Rev.* **2021**, *217*, 4.
- (19) Zong, C.; Xu, M. X.; Xu, L. J.; Wei, T.; Ma, X.; Zheng, X. S.; Hu, R.; Ren, B. *Chem. Rev.* **2018**, *118*, 4946–4980.
- (20) Dulkeith, E.; Morteani, A. C.; Niedereichholz, T.; Klar, T. A.; Feldmann, J.; Levi, S. A.; Veggel, F. C. J. M.; Reinhoudt, D. N.; Möller, M.; Gittins, D. I. *Phys. Rev. Lett.* **2002**, *89*, No. 203002.
- (21) Campion, A.; Ivanecky, J. E., III; Child, C. M.; Foster, M. J. *Am. Chem. Soc.* **1995**, *117*, 11807–11808.
- (22) Dods, R.; Bâth, P.; Morozov, D.; Gagnér, V. A.; Arnlund, D.; Luk, H. L.; Kübel, J.; Maj, M.; Vallejos, A.; Wickstrand, C.; Bosman, R.; Beyerlein, K. R.; Nelson, G.; Liang, M. N.; Milathianaki, D.; Robinson, J.; Harimoorthy, R.; Berntsen, P.; Malmerberg, E.; Johansson, L.; Andersson, R.; Carbajo, S.; Claesson, E.; Conrad, C. E.; Dahl, P.; Hammarin, G.; Hunter, M. S.; Li, C. F.; Lisova, S.; Royant, A.; Safari, C.; Sharma, A.; Williams, G. J.; Yefanov, O.; Westenhoff, S.; Davidsson, J.; DePonte, D. P.; Boutet, S.; Barty, A.; Katona, G.; Groenhof, G.; Brändén, G.; Neutze, R. *Nature* **2021**, *589*, 310–314.
- (23) Wu, K.; Chen, J.; McBride, J. R.; Lian, T. *Science* **2015**, *349*, 632–635.
- (24) Rao, A. M.; Eklund, P. C.; Bandow, S.; Thess, A.; Smalley, R. E. *Nature* **1997**, *388*, 257–259.
- (25) Chen, N.; Xiao, T. H.; Luo, Z. Y.; Kitahama, Y.; Hiramatsu, K.; Kishimoto, N.; Itoh, T.; Cheng, Z. Z.; Goda, K. *Nat. Commun.* **2020**, *11*, 4772.
- (26) Liu, D. H.; Chen, X. S.; Hu, Y. B.; Sun, T.; Song, Z. B.; Zheng, Y. J.; Cao, Y. B.; Cai, Z.; Cao, M.; Peng, L.; Huang, Y. L.; Du, L.; Yang, W. L.; Chen, G.; Wei, D. P.; Wee, A. T. S.; Wei, D. C. *Nat. Commun.* **2018**, *9*, 193.
- (27) Sun, H. Z.; Cong, S.; Zheng, Z. H.; Wang, Z.; Chen, Z. G.; Zhao, Z. G. *J. Am. Chem. Soc.* **2019**, *141*, 870–878.
- (28) Toporski, J.; Dieing, T.; Hollricher, O. *Confocal Raman Microscopy*; Springer International Publishing AG, 2018.
- (29) Yasuda, S.; Takahashi, Y.; Asano, T.; Saito, Y.; Kikunaga, K.; Yamashita, D.; Noda, S.; Takahashi, Y. *Opt. Express* **2021**, *29*, 16228–16240.
- (30) Park, S.; Choe, W.; Lee, H.; Park, J. Y.; Kim, J.; Moon, S. Y.; Cvelbar, U. *Nature* **2021**, *592*, 49–53.
- (31) Fylladitakis, E. D.; Theodoridis, M. P.; Moronis, A. X. *IEEE Trans. Plasma Sci.* **2014**, *42*, 358–375.
- (32) Bittencourt, J. A. *Fundamentals of Plasma Physics*; Springer Science + Business Media, LLC, 2004.
- (33) Vlahovska, P. M. *Annu. Rev. Fluid Mech.* **2019**, *51*, 305–330.
- (34) Park, S.; Cvelbar, U.; Choe, W.; Moon, S. Y. *Nat. Commun.* **2018**, *9*, 371.
- (35) Wang, J.; Zhu, T.; Cai, Y. X.; Zhang, J. F.; Wang, J. B. *Int. J. Heat Mass Transf.* **2020**, *152*, No. 119545.
- (36) Trivedi, D. J.; Barrow, B.; Schatz, G. C. *J. Chem. Phys.* **2020**, *153*, 124706.
- (37) Naujoks, D. *Plasma-Material Interaction in Controlled Fusion*; Springer-Verlag Berlin Heidelberg, 2006.
- (38) Xi, W. J.; Shrestha, B. K.; Haes, A. J. *Anal. Chem.* **2018**, *90*, 128–143.
- (39) Persson, B. N. J.; Zhao, K.; Zhang, Z. Y. *Phys. Rev. Lett.* **2006**, *96*, No. 207401.
- (40) Fang, Y.; Seong, N. H.; Dlott, D. D. *Science* **2008**, *321*, 388–392.
- (41) Jiang, S. Y.; Ma, A.; Ramachandran, S. *Int. J. Mol. Sci.* **2018**, *19*, 2966.
- (42) Teter, D. M.; Hemley, R. J. *Science* **1996**, *271*, 53–55.
- (43) Jiang, J. Z.; Ou-yang, L.; Zhu, L. H.; Zheng, A. M.; Zou, J.; Yi, X. F.; Tang, H. Q. *Carbon* **2014**, *80*, 213–221.
- (44) Miller, T. S.; Jorge, A. B.; Suter, T. M.; Sella, A.; Corà, F.; McMillan, P. F. *Phys. Chem. Chem. Phys.* **2017**, *19*, 15613–15638.
- (45) Lakowicz, J. R. *Principles of Fluorescence Spectroscopy*; Springer Science + Business Media, LLC, 2006.

(46) Shashoua, Y.; Berthelsen, M. B. L. D.; Nielsen, O. F. *J. Raman Spectrosc.* **2006**, *37*, 1221–1227.

(47) Witze, A. *Nature* **2021**, *594*, 484.

(48) Xu, H. F.; He, Y.; Strobel, K. L.; Gilmore, C. K.; Kelley, S. P.; Hennick, C. C.; Sebastian, T.; Woolston, M. R.; Perreault, D. J.; Barrett, S. R. H. *Nature* **2018**, *563*, 532–535.

(49) Zharov, A.; Fierro, V.; Celzard, A. *Appl. Phys. Lett.* **2020**, *117*, 104101.

(50) Bartis, E. A. J.; Knoll, A. J.; Luan, P.; Seog, J.; Oehrlein, G. S. *Plasma Chem. Plasma Process.* **2016**, *36*, 121–149.

Recommended by ACS

Artificial Light-Harvesting System Based on Zinc Porphyrin and Benzimidazole: Construction, Resonance Energy Transfer, and Amplification Strategy for Electrochemilu...

Yi-Xuan Li, Dan Shan, *et al.*

FEBRUARY 03, 2023
ANALYTICAL CHEMISTRY

READ 

Determination of Secondary Structure of Proteins by Nanoinfrared Spectroscopy

Jehan Waeytens, Vincent Raussens, *et al.*

JANUARY 04, 2023
ANALYTICAL CHEMISTRY

READ 

Spectral Unmixing for Label-Free, In-Liquid Characterization of Biomass Microstructure and Biopolymer Content by Coherent Raman Imaging

Simon Vilms Pedersen, Eva Arnsjang Christensen, *et al.*

JANUARY 13, 2023
ANALYTICAL CHEMISTRY

READ 

Protein Dielectrophoresis with Gradient Array of Conductive Electrodes Sheds New Light on Empirical Theory

Siarhei Zavatski, Olivier J. F. Martin, *et al.*

JANUARY 24, 2023
ANALYTICAL CHEMISTRY

READ 

Get More Suggestions >